Appl. Phys. B 65, 453–458 (1997)

Applied Physics B Lasers and Optics

Simulations on false gain in recombination-pumped soft-X-ray lasers

T. Ozaki*, **H. Kuroda**

Institute for Solid State Physics, University of Tokyo, 7-22-1 Roppongi, Minato-Ku, Tokyo 106, Japan

Received: 10 December 1996/Revised version: 12 March 1997

Abstract. Numerical investigations are performed on false gain due to axial plasma expansion, which is expected to be important in initial proof-of-principle studies of recombination-pumped soft-X-ray lasers with extended capabilities. Modelling calculations of experiments with slab boron nitride targets reveal large false gain coefficients approaching $20\,\mathrm{cm}^{-1}$ in the case of plasmas with short active medium lengths. The false gain in the case of fiber targets is found to be of equal magnitude to that for slabs in the case of plasmas with less than 0.1 cm active medium lengths. Calculations for slab targets predict that adopting a tolerance of $\pm 1\,\mathrm{cm}^{-1}$ for gain will severely restrict the time and the active medium length of the plasma that can be used for error-free observations, while those for fiber targets are found to be considerably relaxed. The effects of false gain in the 54.2 Å Na Balmer α laser is also investigated, again revealing the importance of this phenomena under optimum gain conditions.

PACS: 52.25.Nr; 42.55.Vc; 52.50.Jm

Major research goals for soft-X-ray lasers are saturated and large gain-length product operation, shorter wavelengths into the spectral water-window, and demonstrations of lasing with more compact systems. The electron-collisional scheme has been successful in demonstrating saturated soft-X-ray lasers [1–4] and has also been operated at wavelengths just below the carbon K edge at 43.18 Å [5]. The next generation soft-X-ray lasers will aim at realizing lasing at even shorter wavelengths and with much smaller pumps. This will necessitate new and novel pumping methods, requiring further research and investigations into possible mechanisms for achieving such goals. However, for many cases, initial studies and proof-of-principle investigations of soft-X-ray lasers with such extended capabilities will be performed under relatively small gain-length products, and distinguishing between actual and spurious amplifications will be a major concern.

*E-mail: john@ludwig.issp.u-tokyo.ac.jp

The authors have identified experimentally a source of systematic error that can severely overestimate gain coefficients evaluated using elongated plasmas with excessively short active medium lengths [6, 7]. The cause of this error has been identified as being due to plasma expansion in the axial direction, resulting in different cooling rates for plasmas of different lengths. This phenomenon has also been mentioned and dealt with in the work of Shmatov [8]. Experimental observations of spectra from plasmas produced on solid slab targets showed that this phenomena results in a different temporal profile of the spontaneous intensity emitted from plasmas with different active medium lengths, thus resulting in an "apparent" amplification. Time-resolved observations revealed that such deviations became larger with time, resulting in an increase in the magnitude of false gain [6]. Space-resolved observations showed that false gain coefficients also increased with the distance z normal from the target surface for the N Balmer α line exceeding $3\,\mathrm{cm}^{-1}$ at $z \geq 300\,\mu\mathrm{m}$ for plasmas with active medium lengths of 8 mm [9]. Such an error will largely affect the results of gain measurement experiments for soft-X-ray lasers employing relatively short active medium lengths such as the ultra-short pulse pumped recombination lasers [10] and optical-field ionization lasers [11, 12]. It is therefore important that we quantitatively clarify the effects of this systematic error.

In this paper we perform numerical calculations on false gain in recombination-pumped soft-X-ray laser media with the main objective of clarifying its effects under various target and irradiation conditions. In Sect. 1, we perform modelling calculations of experiments using slab boron nitride targets irradiated by pump laser pulses of 100-ps duration . We show the effects of the active medium length on the magnitude of false gain and also reveal the existence of false absorption. The initial conditions obtained in this section are used in Sect. 2 to investigate false gain for fiber targets, which are frequently applied to the recombination scheme. Finally, in Sect. 3, results are presented in which we show the effects of systematic errors for experiments aimed at generating shorter wavelength soft-X-ray lasers, namely the Na Balmer α laser.

1 Modelling of experiments with slab targets

The program used in the present work couples an atomic kinetics code with a hydrodynamics code in order to calculate the temporal change in the spontaneous emission intensities and gain of H-like transitions emitted from an expanding cylindrical plasma [9]. Populations of each ionic state are calculated based on a transient collisional-radiative model [13–16]. Ion species from completely ionized to Li-like ions are included, with the excited states taken into account only for the H-like ion, for levels with principal quantum numbers of $n = 2$–15. Reabsorption of the resonance lines are included in the calculation using the escape probability formulas for cylindrically expanding plasmas [17, 18]. We assume an initial plasma with a cylindrical geometry in our calculations. The hydrodynamic evolution of the plasma is calculated based on a revised self-similar model. In order to include the effects of false gain, we divide the hydrodynamic calculations within a single time increment into two steps. In the first step, radial expansion of the plasma is calculated using the conventional self-similar model [19, 20]. In the next step, expansion of the plasma in the axial direction is calculated by assuming a constant angle Θ between the velocity vector $\boldsymbol{v}$ at the ends of the elongated plasma and its radial component $\boldsymbol{v}_\mathrm{r}$. We employ a parameter $\delta \equiv \tan\Theta$ to represent the magnitude of axial expansion. After the plasma is expanded along the axial direction, the electron and ion densities, n, and temperatures, T, are modified to compensate for the change in the plasma volume, V. We assume the effects of axial plasma expansion to be perturbations and use the adiabatic relation $nV = \text{const.}$ and $TV^{2/3} = \text{const.}$ The numerical accuracy of the calculations is checked by reducing the time increment and confirming that the resulting solutions converge.

In order to simulate experimental results correctly with this relatively simple code, we reproduce the time-resolved spectra of [6] by adjusting the initial conditions of calculation. The first guess is selected such that the calculated spontaneous emission intensity of the H-like N Balmer α line under the condition of $\delta = 0$ (i.e., no expansion in the axial direction of the plasma) is in agreement with the experimentally observed intensity profile for $l = 0.78$ cm. Next, the initial conditions and δ are adjusted such that the observed and calculated spontaneous emission intensities of the N Balmer α line for $l = 0.08$ and 0.16 cm also show agreement. The initial plasma conditions of the calculation obtained in this manner are radius $R_0 = 45$ μm, electron density $N_\mathrm{e} = 10^{21}$ cm^{-3}, electron temperature $T_\mathrm{e} = 140$ eV, and $\delta = 3.0$. This large value of δ can be attributed to the oversimplified model used and may be different from the actual angle of axial expansion. We shall use these initial conditions in order to investigate the various features of false gain under the present experimental conditions.

In Fig. 1 we plot the change in the calculated spectral intensity I of the H-like N Balmer α line as a function of active medium length l for $l = 0.02$–0.8 cm. The data set corresponds to a time $t = 3.0$ nsec from the start of the plasma expansion. We also plot the ratio between I and the spectral intensity I_0 obtained from calculations with $\delta = 0$ (i.e., no axial expansion). Evidently, I_0 is a linear function of l which takes a null value at $l = 0$ cm. We can see from the figure that at $t = 3.0$ nsec, the ratio I/I_0 monotonically decreases with a decrease in l. This nonlinear behaviour of I with active medium length causes what are intrinsically spontaneous emissions to show spurious amplifications. It is interesting to note that the spectral intensity I in Fig. 1 changes from a strongly nonlinear dependence on l for $l \leq 0.2$ cm to an almost linear one for $l \geq 0.3$ cm. The nonlinear characteristic of spontaneous emission for small l implies large errors when using these data points for gain evaluation. Data points for $l \geq 0.3$ cm, on the other hand, fall closely onto a linear fit which intersects the abscissa at $l > 0$ cm. Therefore the magnitude of false gain can be expected to be smaller for this region compared with that at $l \geq 0.2$ cm and, from simple considerations, is found to decrease with an increase in l.

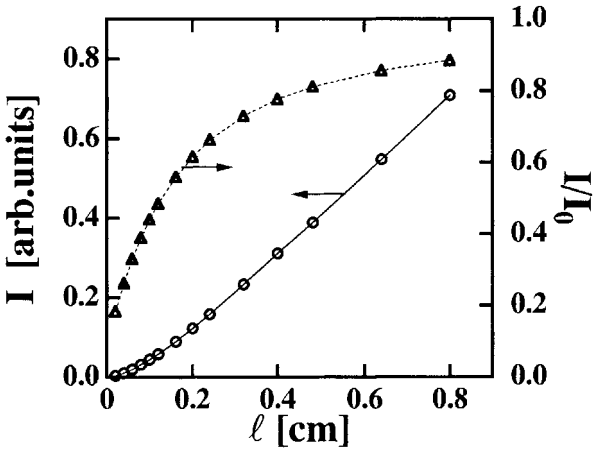

Fig. 1. Spectral intensity I of the N Balmer α line as a function of the active medium length l for $l = 0.02$–0.8 cm and at a time $t = 3.0$ nsec for slab targets. The ratio I/I_0 between I and the spectral intensity Io for null axial expansion is also shown

Next we evaluate from the above data set the magnitude of false gain calculated using various active medium lengths l. It is important to point out here that the value of false gain coefficients obtained from fitting to gain formulas depend on which data points are used. This is because the deviation of I from I_0 due to the effects of axial plasma expansion does not necessarily follow any gain formula. We therefore adopt the same method of selecting data points for gain measurements that are used in our experiments [7] by choosing plasmas with active medium lengths $l = (n/5) \times l_\mathrm{max}$ (where $n = 1$, 2, 3, 4, 5). Here l_max corresponds to the maximum l used in the fitting process. The change in the calculated false gain coefficients with time t, obtained by a least-mean-square fitting procedure to the gain formula of Linford et al. [21], is shown in Fig. 2 for $l_\mathrm{max} = 0.1$, 0.2, 0.4, and 0.8 cm. Large values of false gain of 18.6, 8.5, and 3.3 cm^{-1} occur at $t = 3.0$ nsec for $l_\mathrm{max} = 0.1$, 0.2, and 0.4 cm, respectively. False gain coefficients are found to increase at an especially rapid rate for $l \leq 0.2$ cm, where extremely large systematic errors of greater than 10 cm^{-1} are predicted to be observed. False gain coefficients take an almost constant value for $t > 3.0$ nsec in the case of $l_\mathrm{max} = 0.1$ and 0.2 cm, while those for $l_\mathrm{max} > 0.4$ cm reveal a weak but gradual increase with time. One can also recognize in the figure that false gain is negative for all four cases at $t \leq 2$ nsec. Such negative false gain will give rise to an underestimation of gain coefficients, i.e. false absorption. The absolute magnitude of false absorption is found to be comparable to that of false gain and also rapidly increases with a decrease in l. As was previously mentioned, these false gain coefficients vary

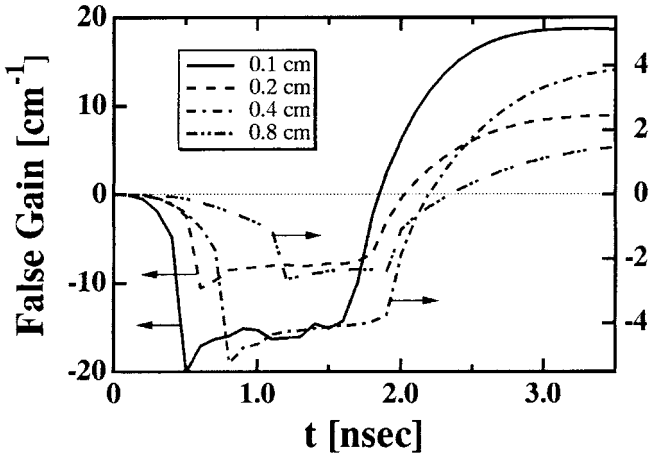

Fig. 2. Change in the calculated false gain coefficients with time t for slab targets and $l_{max} = 0.1$, 0.2, 0.4, and 0.8 cm

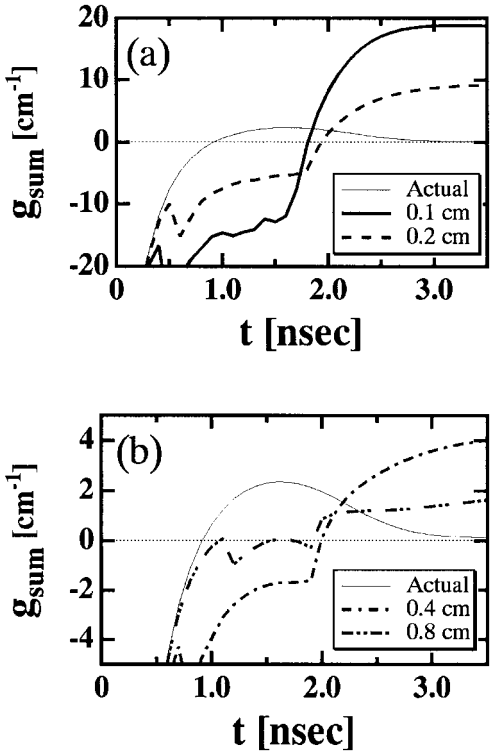

Fig. 3a,b. Sum g_{sum} of the actual and false gain coefficient for slab targets with **a** $l_{max} = 0.1$ and 0.2 cm, and **b** $l_{max} = 0.4$and 0.8 cm, along with the actual gain coefficient for null axial expansion

with the set of data points selected for fitting. For example, for the data set corresponding to $l_{max} = 0.2$ cm, the false gain coefficient decreases to 7.2 cm^{-1} if the smaller two data points at $l = 0.04$ and 0.08 cm are neglected. This decrease in false gain is the result of the monotonic decrease in the ratio I/I_0 with smaller l observed in Fig. 1.

The effects of false gain also depend on its magnitude relative to that of the actual gain coefficient. We therefore plot in Fig. 3 the sum of the actual and false gain for $l_{max} = 0.1$, 0.2, 0.4, and 0.8 cm, along with the actual gain coefficient for null axial expansion. We can see that the peak of the actual gain profile centered at $t = 1.6$ nsec disappears under the

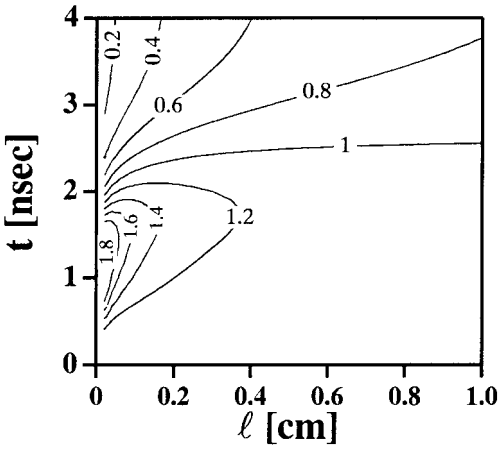

Fig. 4. Contour plot of the ratio I/I_0 for slab targets as a function of l and t

effects of systematic errors due to false absorption observed before $t = 2.0$ nsec. False gain also dominates the total gain for $t \geq 2.0$ nsec, resulting in a prolonged gain profile continuing long after $t = 3.5$ nsec. The calculated gain profile of the N Balmer α line for $l_{max} = 0.8$ cm shown in this figure compares extremely well with that obtained from experiments with $l_{max} = 0.78$ cm [22]. Observations of the plasma at a position 200 μm normal from the target surface showed an approximately zero gain for $t \leq 2.1$ nsec, which then increased to 2 cm^{-1} at $t = 2.4$ nsec. Gain coefficients could not be evaluated from experimental data for $t \leq 2.5$ nsec owing to the low spectral intensities with relatively small l.

The cause of false gain and false absorption are both the results of the different rate at which the plasma expands and cools for different l. The enhanced rate at which the electron density decays for plasmas with reduced l is due to the smaller total volume of such plasma, which will cause axial expansion to have a larger influence on the expansion rate compared with plasmas possessing longer active medium lengths. In the case of plasma conditions relevant to recombination pumped soft-X-ray lasers, a faster cooling of the plasma will initially cause an enhanced pumping of the upper laser level, because three-body recombination becomes dominant earlier, when a larger abundance of the fully ionized ions exists. This will result in an initial increase in the population of the upper laser level, and thus an increase in the spontaneous emission intensity per unit length for plasmas with shorter active media lengths, consequently causing false absorptions to be observed. There is a possibility that for small l the actual population inversion and gain might be enhanced due to such enhancements in the cooling rate of the plasma. Nevertheless, the prerequisite that plasma conditions must be identical for the various data used in gain measurements is not satisfied, and therefore it would be misleading to employ plasmas with excessively small l.

In Fig. 4, we show the contour plot of the ratio I/I_0 under the present calculation conditions as a function of l and t. A contour line corresponding to unity ratio can be observed at around $t = 2$ nsec. For smaller times the intensity ratios are greater than unity and I/I_0 is found to increase monotonically with decreasing l. A region with an exceptionally high ratio can be observed for $l \leq 0.2$ cm between $t = 0.5$ and 1.5 nsec. In such regions, the spectral intensity for data points with

small l will appear enhanced and the plot of intensity against l will be typical of those for transitions with negative gain. For times exceeding $t = 2$ nsec, the I/I_0 ratio becomes less than unity. In this region, the ratio monotonically decreases with a decrease in l and a switch from false absorption to false amplification is observed.

Next, we evaluate false gain coefficients from the above data set. For l_{max} we selected ten data points between 0.1 and 1.0 cm. In the same manner as before, five data points are chosen for fitting with $l = (n/5) \times l_{max}$ ($n = 1, 2, 3, 4, 5$). The contour lines corresponding to false gain coefficients between -5 and 5 cm^{-1} obtained in this manner are shown in Fig. 5. Results show false absorption coefficients before $t = 2$ nsec, even for a relatively long plasma of $l_{max} = 1.0$ cm. The contour line corresponding to zero error lies around $t = 2$ nsec, after which considerable false gain prevails. Again, the region at which false gain can be ignored is severely limited. For example, if we restrict the maximum allowed false gain to be ± 11 cm^{-1}, gain measurements for $l_{max} = 1.0$ cm data are allowed only at $t \leq 1.2$ nsec and $2.0 \leq t \leq 3.2$ nsec. Applying the same tolerance to $l_{max} = 0.5$ cm data will further limit measurements to $t \leq 0.7$ nsec and $2.0 \leq t \leq 2.4$ nsec.

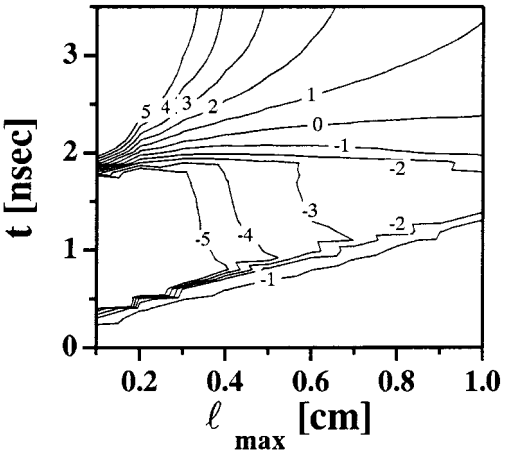

Fig. 5. Contour lines corresponding to false gain coefficients between -5 and 5 cm^{-1} for slab targets at an initial electron temperature of 140 eV

2 False gain with fiber targets

In the preceding section, we performed modelling calculations which clarified the effects of false gain in experiments employing slab targets. Another target geometry that is often used for soft-X-ray lasers, especially with recombination pumped schemes, is the thin fiber target. It is therefore important to know how significant false gain effects are associated with such target geometries as compared with slabs. In this section, we investigate the effects of systematic errors in gain evaluation experiments for fiber targets, assuming an initial plasma radius of $R_0 = 5$ μm. The initial conditions of calculations other than R_0 are kept equal to those used in the preceding section, i.e. $n_e = 10^{21}$ cm^{-3}, $T_e = 140$ eV, and $\delta = 3.0$.

In Fig. 6, we show a contour plot of I/I_0 for the 5 μm radius fiber targets as a function of l and t. Under the present condition, the ratio is unity at around $t = 0.3$ nsec and a narrow region exists centered at 0.2 nsec for small l where I/I_0 is greater than 1.2. The region where the intensity ratio becomes less than 0.8 is also limited to small l as compared with those for slab targets. A comparison of Fig. 6 with Fig. 4 will give the impression that false gain is of little importance for thin fiber targets. This, however, is not necessarily the case, which can be seen from the plot of false gain with fiber targets as a function of time for $l_{max} = 0.1$, 0.2, 0.4, and 0.8 cm as shown in Fig. 7. The magnitude of false absorption is comparable to that of slabs in the case of $l_{max} = 0.1$ cm plasmas, and coefficients exceeding -20 cm^{-1} can be observed for $t > 0.2$ nsec. False gain, on the other hand, is approximately half of that observed with slab targets under the present calculation condition and the change with time for $t \geq 0.6$ nsec is small. Both false gain and absorption are found to decrease rapidly with an increase in l_{max}. The relatively large systematic error observed for fibers with small l_{max} is a result of the rapid change in the intensity ratio I/I_0 for $l \leq 0.1$ cm. As I_0 is a linear function of the active medium length intersecting the abscissa at $l = 0$ cm, the magnitude of false gain is directly

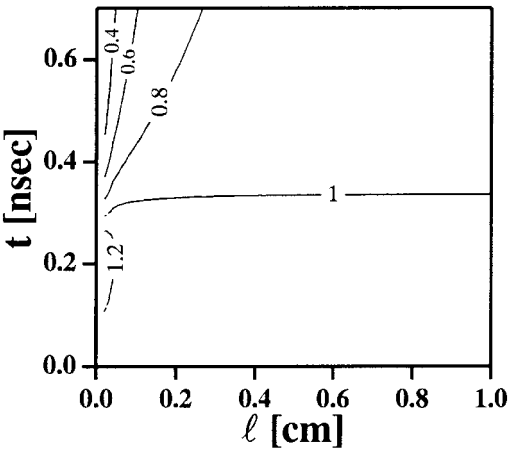

Fig. 6. Contour plot of the intensity ratio I/I_0 as a function of l and t for fiber targets

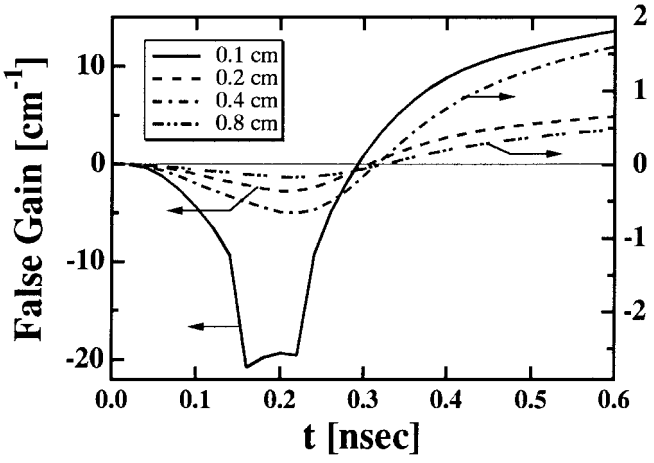

Fig. 7. Plot of false gain as a function of time t for $R_0 = 5$ μm fiber targets with $l_{max} = 0.1$, 0.2, 0.4, and 0.8 cm

related to the rate of change of I/I_0 with l, and not on the absolute value of the intensity ratio. Therefore, regions in Fig. 6 where the contour lines are closely spaced correspond to conditions where false gain (when $I/I_0 < 1$) or false absorption (when $I/I_0 > 1$) are large. Compared with the results of slab

targets, the contour lines for fiber targets are broadly spaced for $l \geq 0.2$ cm, resulting in the rapid decrease in errors with an increase in l_{max}.

The real gain coefficient for the N Balmer α line is found to be maximum for an initial electron temperature of 100 eV. In Fig. 8, we show the contour plot of false gain coefficients evaluated for fiber targets at this optimum initial electron temperature. The boundary for false gain coefficients of 1 cm^{-1} is at $t = 0.6$ nsec for $l_{max} = 0.6$ cm, while false absorption of -1 cm^{-1} can only be observed for $l_{max} < 0.4$ cm. Results given in Fig. 8 thus suggests insignificant effects of axial plasma expansion when using data sets with $l_{max} \geq 0.6$ cm for fiber targets with $R_0 = 5$ μm and initial electron temperatures of 100 eV. However, simulations show that the region of false gain tends to extend to larger l with an increase in the initial electron temperature. It is therefore possible that irradiation of fiber targets at excessively high peak intensities will result in a considerable systematic error in the gain coefficient for even larger l.

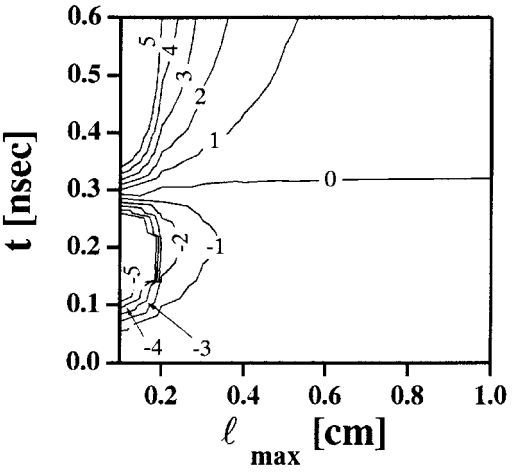

Fig. 8. Contour lines corresponding to false gain coefficients between -5 and 5 cm^{-1} for N fiber targets at an initial electron temperature of 100 eV

3 False gain for shorter wavelength soft-X-ray lasers

Simulations show that an increase in the initial electron temperature will extend the effects of large systematic errors to plasmas with longer active medium lengths, which also start from an earlier time. This becomes of great concern when performing recombination pumped soft-X-ray laser experiments with shorter wavelengths into, for example, the spectral water-window. Such systems will employ targets with larger atomic numbers and therefore will require higher initial electron temperatures to attain the initial ionization stage necessary for the shorter wavelength. In order to investigate the effects of false gain in such soft-X-ray lasers, we performed modelling calculations of the 54.2 Å Na Balmer α laser.

In Fig. 9 we show the contour plot of the calculated false gain between -5 and 5 cm^{-1} for slab Na targets. The initial conditions for these calculations are $N_e = 10^{21}$ cm^{-3}, $T_e = 350$ eV, $R_0 = 45$ μm, and $\delta = 3.0$; these are selected so that the actual gain coefficient of the Na Balmer α line without axial plasma expansion becomes a maximum. Results reveal a drastic reduction in the effects of false absorption compared with those for N slab targets. False absorption coefficients are less than 1 cm^{-1} for $l_{max} \geq 0.4$ cm, as compared with the results for N slabs, where false absorption greater than 1 cm^{-1} can be observed in Fig. 5 even for $l_{max} \leq 1.0$ cm. False gain can, on the other hand, still be of importance for Na targets. For example, false gain coefficients exceed 1 cm^{-1} at $t = 1.9$ nsec for $l_{max} = 1.0$ cm, at which time the normalized spontaneous emission intensity of the Na Balmer α line is still 0.24.

The contour plot of false gain for 5 μm radius fiber Na targets is shown in Fig. 10 for initial conditions of $n_e = 10^{21}$ cm^{-3}, $T_e = 350$ eV, and $\delta = 3.0$. This electron temperature is also selected so that the actual gain of the Na Balmer α line at $\delta = 0$ is maximum. The contour plot for Na and N fiber targets under optimum plasma conditions for gain show a good resemblance, if we multiply the time scale of Fig. 10 by a factor of two. The normalized spontaneous emission intensity for Na and N Balmer α lines are both equal to 0.2 at $t = 0.3$ and 0.6 nsec, respectively, justifying the above comparison. In fact, the contour plot of false gain for slab N and

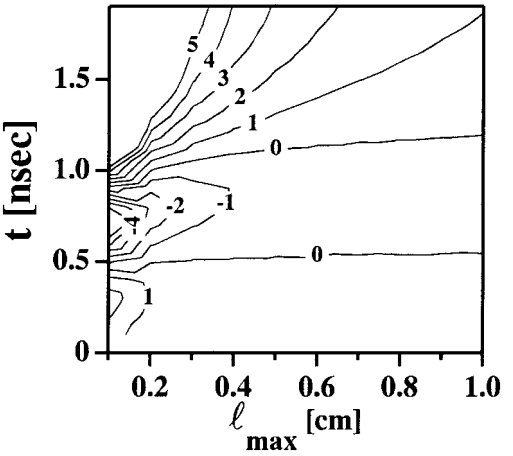

Fig. 9. Contour lines corresponding to false gain coefficients between -5 and 5 cm^{-1} for Na slab targets. The initial conditions of calculation are $n_e = 10^{21}$ cm^{-3}, $T_e = 350$ eV, $R_0 = 45$ μm, and $\delta = 3.0$

Na targets also show a good comparison if we again multiply the time scale of the latter by a factor of two, and neglect contour lines for false absorption. This similarity in the contour plot of false gain coefficients for soft-X-ray laser media with different atomic number Z can be attributed to a balance between the shorter time scale of emission for soft-X-ray lasers with larger Z and the shift of the contour lines of false gain to larger l and smaller t with an increase in the required initial electron temperature of the plasma. Thus, the effects of false gain in conventional recombination pumped soft-X-ray lasers are found to be of an approximately equal significance irrespective of the operating wavelength.

4 Conclusion

In conclusion, we present results of numerical investigations on false gain in soft-X-ray laser media due to axial plasma expansions. Modelling calculations of experiments with slab boron nitride targets reveal large false gain coefficients exceeding 8 cm^{-1} for long times in the case of plasmas with an active medium length of less than 0.2 cm. The presence

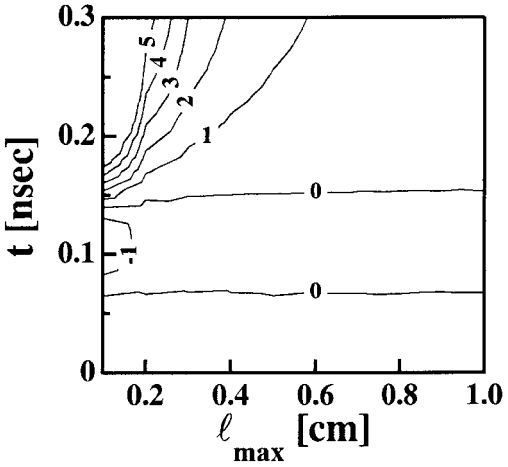

Fig. 10. Contour lines corresponding to false gain coefficients between -5 and $5\,\mathrm{cm}^{-1}$ for Na fiber targets. The initial conditions of calculation are $n_\mathrm{e} = 10^{21}\,\mathrm{cm}^{-3}$, $T_\mathrm{e} = 350\,\mathrm{eV}$, $R_0 = 5\,\mu\mathrm{m}$, and $\delta = 3.0$

of a negative false gain or false absorption is revealed in the early stage of expansion. Observed gain coefficients of the N Balmer α line is found to be well explained by including the effects of such systematic errors in the calculations. The initial conditions obtained from these modelling calculations are used to investigate the effects of similar errors in N fiber targets. False gain in fiber targets is found to be of equal magnitude to that for slabs, which is, however, restricted to plasmas with less than 0.1 cm active medium lengths. Calculations predict that for slab targets a tolerance in the systematic error corresponding to $\pm 1\,\mathrm{cm}^{-1}$ will severely restrict the time and the active medium length of the plasma that can be used for error-free observations, while those in the case of fiber targets are considerably relaxed. We also performed numerical calculations of the 54.2 Å Na Balmer α laser to investigate the effects of false gain on shorter wavelength soft-X-ray lasers. The contour plots of false gain for the N and Na Balmer α lasers showed a good resemblance under optimum gain conditions. This is explained as being due to a balance between an enhanced decay of spontaneous emission and the shift in the magnitude of error to earlier times and shorter active medium lengths with an increase in the atomic number of the lasing ion. As a result, the effects of false gain in conventional recombination pumped soft-X-ray lasers are found to be of an approximately equal significance irrespective of the operating wavelength.

References

1. A. Carillon, H.Z. Chen, P. Dhez, L. Dwivedi, J. Jacoby, P. Jaegle, G. Jamelot, Jie Zhang, M.H. Key, A. Kidd, A. Klisnick, R. Kodama, J. Krishnan, C.L.S. Lewis, D. Neely, P. Norreys, D.O'Neill, G.J. Pert, S.A. Ramsden, J.P. Raucourt, G.J. Tallents, J. Uhomoibhi: Phys. Rev. Lett. **68**, 2917 (1992)
2. S. Wang, Y. Gu, G. Zhou, S. Yu, S. Fu, Y. Ni, J. Wu, Z. Zhou, G. Han, Z. Tao, Z. Lin, S. Wang, W. Chen, D. Fan, G. Zhang, J. Sheng, H. Peng, T. Zhang, Y. Shao: J. Opt. Soc. Am. B **9**, 360 (1992)
3. C.L.S. Lewis, D. Neely, D.M. O'Neill, J.O. Uhomoibhi, M.H. Key, Y. Al Hadithi, G.J. Tallents, S.A. Ramsden: Opt. Commun. **91**, 71 (1992)
4. L.B. Da Silva, B.J. MacGowan, S. Mrowka, J.A. Koch, R.A. London, D.L. Matthews, J.H. Underwood: Opt. Lett. **18**, 1174 (1993)
5. B.J. MacGowan, S. Maxon, L.B. Da Silva, D.J. Fields, C.J. Keane, D.L. Matthews, A.L. Osterheld, J.H. Scofield, G. Shimkaveg, G.F. Stone: Phys. Rev. Lett. **65**, 420 (1990)
6. T. Ozaki, H. Kuroda: Phys. Rev. E **51**, R24 (1995)
7. T. Ozaki, H. Kuroda: J. Opt. Soc. Am. B **12**, 1338 (1995)
8. M.L. Shmatov: Opt. Spektr. **81**, 372 (1996)
9. T. Ozaki, H. Kuroda: J. Opt. Soc. Am. B **13**, 1873 (1996)
10. J. Zhang, M.H. Key, P.A. Norreys, G.J. Tallents, A. Behjat, C. Danson, A. Demir, L. Dwivedi, M. Holden, P.B. Holden, C.L.S. Lewis, A.G. MacPhee, D. Neely, G.J. Pert, S.A. Ramsden, S.J. Rose, Y.F. Shao, O. Thomas, F. Walsh, Y.L. You: Phys. Rev. Lett. **74**, 1335 (1995)
11. Y. Nagata, K. Midonkawa, S. Kubodera, M. Obara, H. Tashiro, K. Toyoda: Phys. Rev. Lett. **71**, 3774 (1993)
12. B.E. Lemoff, G.Y. Yin, C.L. Gordon III, C.P.J. Barty, S.E. Harris: Phys. Rev. Lett. **74**, 1574 (1995)
13. N. Nakano, H. Kuroda: Phys. Rev. A **27**, 2168 (1983)
14. N. Nakano, H. Kuroda: Phys. Rev. A **29**, 3447 (1984)
15. N. Nakano, H. Kuroda: Appl. Phys. Lett. **45**, 130 (1984)
16. M. Itoh, T. Yabe, S. Kiyokawa: Phys. Rev. A **35**, 233 (1987)
17. A.C. Shestakov, D.C. Eder: J. Quant. Spectrosc. Radiat. Transf. **42**, 483 (1989)
18. D.C. Eder, H.A. Scott: J. Quant. Spectrosc. Radiat. Transf. **45**, 189 (1991)
19. J.M. Dawson: Phys. Fluids **7**, 981 (1964)
20. C.H. Nam, E. Valeo, S. Suckewer, U. Feldman: J. Opt. Soc. Am. B **3**, 1199 (1986)
21. G.J. Linford, E.R. Peressini, W.R. Sooy, M.L. Spaeth: Appl. Opt. **13**, 379 (1974)
22. T. Ozaki, H. Kuroda: Opt. Quantum Electron. **28**, 187 (1996)